

# Tests of the Eigenstate Thermalization Hypothesis in a One-Dimensional Isolated Quantum System

Gregor Krzmarc

Stanford University

`gregork@stanford.edu`

## Abstract

The Eigenstate Thermalization Hypothesis (ETH) provides a microscopic explanation for thermalization in isolated quantum systems [3]. It posits that for chaotic (non-integrable) Hamiltonians, individual energy eigenstates yield expectation values consistent with microcanonical ensemble predictions, whereas integrable systems do not. We test the Eigenstate Thermalization Hypothesis (ETH) using exact diagonalization (ED) on both an integrable and a chaotic 1D XXZ spin chain system. We break the integrability by introducing next-nearest neighbour couplings and a random longitudinal magnetic field. The hypothesis is tested by comparing distributions of energy level spacings, as well as looking at the dependence of expectation values of different operators for different eigenstates and their energies. We also compare the predictions of a microcanonical ensemble for expectation values of operators and the predictions of long-time quantum mechanical expectation values.

## 1 Introduction

Understanding how isolated many-body quantum systems approach equilibrium is an essential question in modern quantum physics. Unlike classical systems, where ergodicity and chaos lead to thermalization in a conceptually transparent way, the mechanism by which a closed quantum system—evolving

unitarily under the Schrödinger equation—can exhibit thermal behavior is far less obvious. A key insight in this direction is the *Eigenstate Thermalization Hypothesis* (ETH), first formulated by Srednicki [3]. ETH proposes that individual energy eigenstates of a quantum many-body Hamiltonian already encode thermal properties, in the sense that the expectation values of observables in a single eigenstate match predictions of thermodynamic ensembles.

## 2 The Eigenstate Thermalization Hypothesis

ETH claims the following for isolated non-integrable, chaotic quantum systems [3, 5]:

1. The diagonal matrix elements of a local observable  $\hat{O}$  in the energy eigenbasis,  $O_{\alpha\alpha} = \langle E_\alpha | \hat{O} | E_\alpha \rangle$ , vary smoothly as a function of energy ( $a_{\hat{O}}(E)$ ) and coincide with microcanonical ensemble predictions.
2. The off-diagonal elements  $O_{\alpha\beta}$  for  $\alpha \neq \beta$  are exponentially small in system size and behave like random variables with a variance determined by the thermodynamic entropy.

Let's define the long-time quantum mechanical average of an observable  $A$  as

$$\langle A \rangle_\infty = \lim_{T \rightarrow \infty} \frac{1}{T} \int_0^T \langle A(t) \rangle dt. \quad (1)$$

Expanding the initial state in the energy eigenbasis as  $|\psi_0\rangle = \sum_\alpha c_\alpha |E_\alpha\rangle$  and using  $A_{\alpha\beta} = \langle E_\alpha | A | E_\beta \rangle$ , the time-dependent expectation value reads

$$\langle A(t) \rangle = \sum_{\alpha, \beta} c_\alpha^* c_\beta A_{\alpha\beta} e^{i(E_\alpha - E_\beta)t}. \quad (2)$$

The time average eliminates all oscillatory off-diagonal terms because

$$\lim_{T \rightarrow \infty} \frac{1}{T} \int_0^T e^{i(E_\alpha - E_\beta)t} dt = \delta_{\alpha\beta}, \quad (3)$$

so that the long-time value reduces to

$$\langle A \rangle_\infty = \sum_\alpha |c_\alpha|^2 A_{\alpha\alpha}. \quad (4)$$

Thus,  $\langle A \rangle_\infty$  represents the stationary value of a quantum mechanical observable  $A$  after a long period of time.

The ETH tells us that after a quench from a non-eigenstate initial condition, long-time averages of observables for a chaotic quantum system reproduce thermal ensemble values:

$$\langle A \rangle_\infty \approx \langle A \rangle_\beta = \frac{\int dE \rho(E) a(E) e^{-\beta E}}{\int dE \rho(E) e^{-\beta E}}.$$

In this expression,  $\beta$  is not an arbitrary parameter. Instead, it is chosen such that the canonical ensemble has the same average energy as the initial state,

$$\langle E \rangle_\beta = E_0, \quad E_0 = \langle \psi_0 | H | \psi_0 \rangle. \quad (5)$$

Thus,  $\beta$  represents the *effective inverse temperature* at which the thermal ensemble reproduces the system's energy.

A crucial distinction arises between *chaotic* and *integrable* systems. Integrable systems possess an extensive set of conserved quantities, which constrains their dynamics and invalidates ETH. Instead of thermalizing, these systems relax to a generalized Gibbs ensemble (GGE) [4]. Quantum chaotic systems, by contrast, typically obey ETH and exhibit signatures of Wigner-Dyson level statistics according to random matrix theory (RMT). This connection between chaos and thermalization is reflected in the distribution of neighboring energy spacings, which we will investigate, among with other diagnostics.

### 3 Random Matrix Theory and the Gaussian Orthogonal Ensemble

Random Matrix Theory (RMT) provides a universal description of energy-level statistics in quantum systems whose classical or many-body dynamics are chaotic. A central result in RMT is that Hamiltonians drawn from ensembles of large random matrices exhibit universal spectral correlations that don't depend on microscopic details. This universality allows one to classify quantum Hamiltonians into symmetry classes whose level statistics match those of corresponding random matrix ensembles. [1]

If we have a real-valued Hamiltonian with time-reversal symmetry, we can model the Hamiltonian as a member of the Gaussian Orthogonal Ensemble (GOE) [1].

Beyond symmetry classification, RMT provides precise predictions for the statistical properties of eigenvalues in chaotic quantum systems. In particular, the distribution of spacings between adjacent energy levels is one of the most sensitive diagnostics of quantum chaos. For a Hamiltonian in the GOE universality class, the nearest-neighbor spacing distribution is given by the Wigner–Dyson form,

$$P_{\text{GOE}}(s) = \frac{\pi}{2} s e^{-\pi s^2/4}, \quad (6)$$

which exhibits the characteristic *level repulsion*  $P(s) \sim s$  as  $s \rightarrow 0$ . This linear suppression of small spacings reflects the fact that energy levels in chaotic systems avoid crossing unless enforced by symmetry [1].

In integrable systems, the presence of an extensive number of mutually commuting conserved quantities partitions the spectrum into many independent subsectors, leaving the energies essentially uncorrelated. As a result, adjacent energy levels do not repel, and the spacing distribution follows Poisson statistics, in contrast to the level repulsion characteristic of chaotic (non-integrable) systems [1].

Their level spacings follow the exponential (Poisson) distribution,

$$P_{\text{Poisson}}(s) = e^{-s}, \quad (7)$$

which has no level repulsion and is peaked at  $s = 0$ . This stark qualitative difference between Poisson and Wigner–Dyson statistics provides a powerful tool for distinguishing integrable and chaotic phases.

An alternative and widely used statistic is the ratio of adjacent level gaps,

$$r_\alpha = \frac{\min(\delta_\alpha, \delta_{\alpha+1})}{\max(\delta_\alpha, \delta_{\alpha+1})}, \quad \delta_\alpha = E_{\alpha+1} - E_\alpha. \quad (8)$$

This ratio has universal averages:

$$\langle r \rangle_{\text{Poisson}} \approx 0.386, \quad \langle r \rangle_{\text{GOE}} \approx 0.530, \quad (9)$$

providing a clean numerical benchmark for the onset of chaos. [5]

## 4 1D XXZ spin chain

In this work we study a spin- $\frac{1}{2}$  XXZ chain including next-nearest-neighbor couplings and a spatially inhomogeneous longitudinal field. The Hamiltonian acting on a chain of length  $L$  is

$$H = \sum_{i=1}^{L-1} \left[ \frac{J}{2} (S_i^+ S_{i+1}^- + S_i^- S_{i+1}^+) + J\Delta S_i^z S_{i+1}^z \right] + \sum_{i=1}^L h_i S_i^z \quad (10)$$

$$+ \sum_{i=1}^{L-2} \left[ \frac{J_2}{2} (S_i^+ S_{i+2}^- + S_i^- S_{i+2}^+) + J_2 S_i^z S_{i+2}^z \right]. \quad (11)$$

Here  $S_i^{x,y,z}$  are spin- $\frac{1}{2}$  operators and  $S_i^\pm = S_i^x \pm iS_i^y$ . The nearest-neighbor terms in Eq. (10) consist of an  $XY$  ‘flip-flop’ exchange, together with an Ising interaction of anisotropy  $\Delta$ . The longitudinal field  $h_i$  may vary from site to site.

Let’s investigate the Hamiltonian. If  $h_i = 0$  for each site  $i$  and  $J_2 = 0$ , the model reduces to a ‘usual’ XXZ spin- $\frac{1}{2}$  chain

$$H_{XXZ} = \sum_{i=1}^{L-1} \left[ \frac{J}{2} (S_i^+ S_{i+1}^- + S_i^- S_{i+1}^+) + J\Delta S_i^z S_{i+1}^z \right]. \quad (12)$$

Such a model is integrable, i.e., carries an extensive set of conserved quantities [2]. We can map such a system via the Jordan-Wigner transformation to a system of interacting spinless fermions [5]. We introduced the  $J_2$  and  $h_i$  terms in order to break integrability and study the properties of the chaotic Hamiltonian.

Let’s try to understand qualitatively what the  $J_2$  and  $h_i$  terms do. If the next-nearest-neighbor coupling  $J_2$  becomes very large,  $J_2 \gg J, h_i$ , the dominant interactions connect spins separated by two lattice sites. In this limit the chain effectively decomposes into two almost independent XXZ subchains formed by the even and odd sites. Such an approximate decoupling introduces additional quasi-conserved quantities, so we don’t expect ETH to hold in this regime.

If instead the longitudinal fields are very large,  $h_i \gg J, J_2$ , the eigenstates become close to product states in the  $S^z$  basis, with interactions providing only weak perturbative corrections, so we would also not expect to see ETH-

consistent results in this case.

## 5 Results

### 5.1 Resolving translation and reflection symmetries

We choose open boundary conditions instead of periodic boundary conditions to break translation symmetry.

By setting  $h_i = 0$  but  $J_2 \neq 0$ , reflection invariance  $R : i \rightarrow L - i - 1$  still remains a symmetry of the Hamiltonian. We break this symmetry by including a small magnetic field at site 0, i.e.  $H \rightarrow H + \epsilon S_0^Z$  with  $\epsilon = 0.1$ . We discuss this further in Appendix A.

### 5.2 Conservation of total magnetization

Hamiltonian 10 commutes with the total z-axis magnetization operator  $S_{tot}^z = \sum_{i=0}^{N+1} S_i^z$ :

$$[H, S_{tot}^z] = 0. \quad (13)$$

Let's verify this: First we look at terms that are diagonal in the  $S^z$  basis: nearest-neighbor and next-nearest-neighbor Ising interactions and the longitudinal field. Using the fact that all  $S_i^z$  commute with one another, we have

$$[S_{tot}^z, S_i^z S_j^z] = \sum_k [S_k^z, S_i^z S_j^z] = 0, \quad (14)$$

for any sites  $i, j$ , and similarly

$$[S_{tot}^z, S_i^z] = 0. \quad (15)$$

Therefore

$$[S_{tot}^z, J\Delta \sum_i S_i^z S_{i+1}^z + J_2 \sum_i S_i^z S_{i+2}^z + \sum_i h_i S_i^z] = 0. \quad (16)$$

Now consider a single nearest-neighbor exchange term  $S_i^+ S_{i+1}^-$ . We com-

pute

$$[S_{\text{tot}}^z, S_i^+ S_{i+1}^-] = \sum_k [S_k^z, S_i^+ S_{i+1}^-] = [S_i^z, S_i^+ S_{i+1}^-] + [S_{i+1}^z, S_i^+ S_{i+1}^-] \quad (17)$$

$$= ([S_i^z, S_i^+]) S_{i+1}^- + S_i^+ ([S_{i+1}^z, S_{i+1}^-]) \quad (18)$$

$$= (+S_i^+) S_{i+1}^- + S_i^+ (-S_{i+1}^-) = 0. \quad (19)$$

An identical calculation shows

$$[S_{\text{tot}}^z, S_i^- S_{i+1}^+] = 0. \quad (20)$$

Since the nearest-neighbor exchange term is a sum of such operators,

$$\left[ S_{\text{tot}}^z, \sum_i \frac{J}{2} (S_i^+ S_{i+1}^- + S_i^- S_{i+1}^+) \right] = 0. \quad (21)$$

Similar reasoning to nearest neighbours applies to the next-nearest-neighbor exchange term (the  $J_2$  term).

Therefore, the Hamiltonian conserves the total number of  $z$ -axis aligned spins. Thus, when simulating our system, we can restrict ourselves to a sector with fixed magnetization in the  $z$ -direction. Similarly to [5], we restrict ourselves to the total magnetization sector of 0, i.e.  $S_z^{tot.} = 0$  with  $\lfloor \frac{L}{2} \rfloor$  spins flipped up. The basis is thus  $\binom{L}{\lfloor L/2 \rfloor}$ -dimensional.

We use open boundary conditions (OBC) and sample per site  $h_i \sim \text{Uniform}[-h_{\text{rand}}, h_{\text{rand}}]$  for a parameter  $h_{\text{rand}} \geq 0$ .

### 5.3 Next nearest-neighbour flip term

Figure 1 shows a gradual emergence of Wigner-Dyson statistics as we increase the next nearest-neighbour coupling term from zero, demonstrating a transition from an integrable system at  $J_2 = 0$  to a chaotic system at  $J_2 = 1$ .

### 5.4 Average $r$ test and the Wigner-Dyson statistics

By systematically exploring the space spanned by both  $J_2$  and  $h_{\text{rand.}}$ , we can identify two regimes: the chaotic one with  $\langle r \rangle \approx 0.53$  and the integrable one

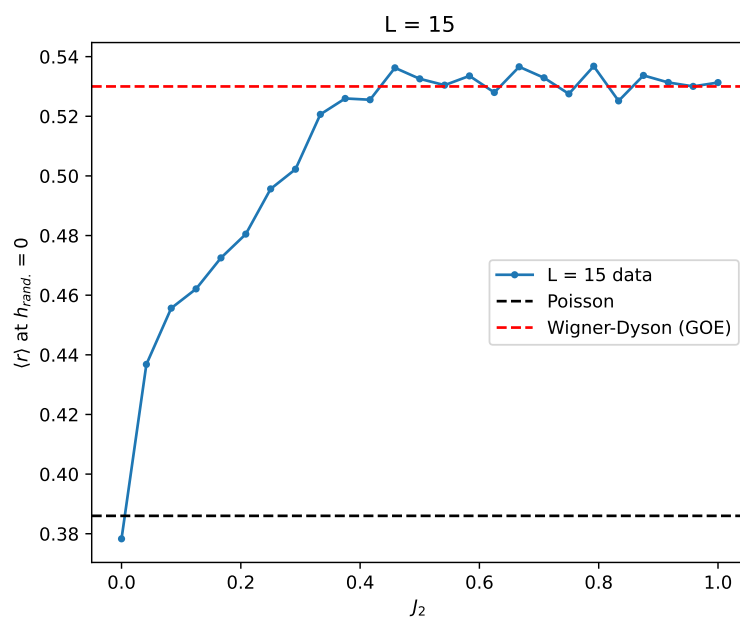


Figure 1: The dependence of  $\langle r \rangle$  on the  $J_2$  term for  $h_{rand} = 0$ , for a chain of size 15. We can observe Poisson statistics with  $\langle r \rangle \approx 0.386$  at  $J_2 = 0$  and Wigner-Dyson statistics at  $\langle r \rangle \approx 0.53$  at  $J_2 \rightarrow 1$ .

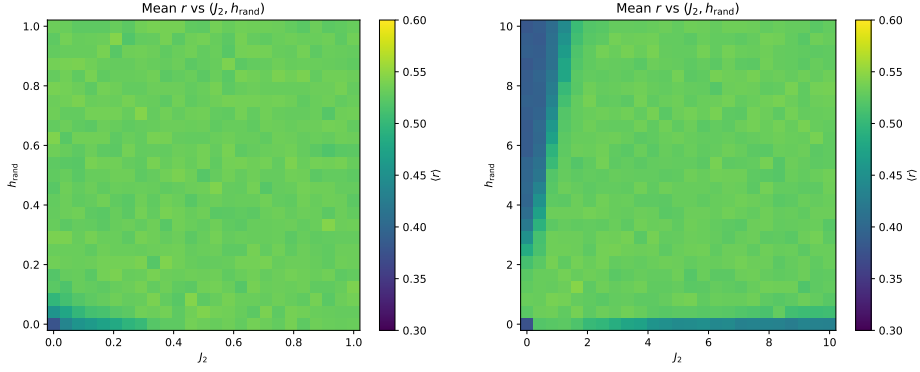


Figure 2: Mean normalized spacing ratio  $r$  for various parameters  $h_{rand}$  and  $J_2$ , for a chain of size  $L = 15$ . The left plot displays a narrower range of the parameters than the right plot. The integrable regime begins when both parameters are close to zero, or when either parameter is large.

with  $\langle r \rangle \approx 0.38$ . There is a smooth transition between the two regimes, as seen from Figure 2. The smooth transition between the regimes is consistent with results obtained for a slightly different XXZ spin chain by [5].

The results at large  $J_2$  but small  $h_{rand}$  as well as a large  $h_{rand}$  and small  $J_2$  are consistent with what we expect from Chapter 4.

## 5.5 Operator expectation values

The ETH predicts that expectation values of operators for eigenstates vary smoothly with the energy of each eigenstate. To verify this, we pick a point from Figure 2 deep in the chaotic regime with  $J_2 = 2$ ,  $h_{rand} = 2$ , and compute expectation values of different operators.

We choose two local and two global operators:

- $S_{L/2}^z$ , the Z-component of the spin at half-length (site  $\lfloor \frac{L}{2} \rfloor$ )
- $S_{L/2}^z S_{L/2+1}^z$ , the "nearest-neighbour bond operator" at half-length
- $T = \frac{1}{N} \sum_{i=1}^{N-2} (S_i^x S_{i+2}^x + S_i^y S_{i+2}^y)$  (similar to [5])
- $Z = \frac{1}{N} \sum_{i=1}^{N-1} S_i^z S_{i+1}^z$ , the average nearest-neighbour bond operator (similar to [5])

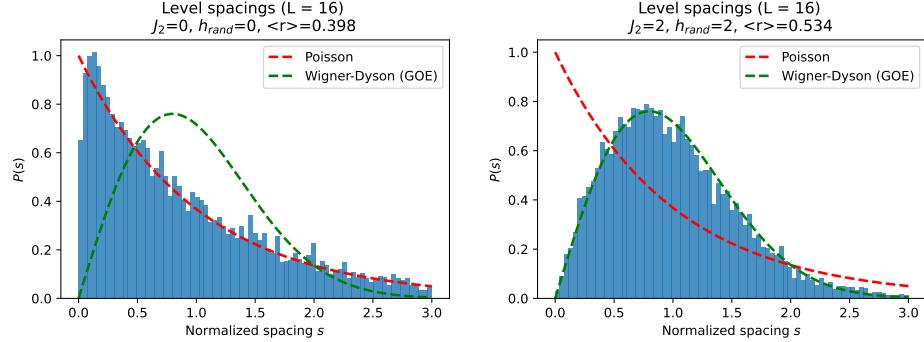


Figure 3: Distribution of normalized energy level spacings  $P(s)$  for the integrable case  $J_2 = 0$ ,  $h_{rand} = 0$  (left) and the chaotic case  $J_2 = 2$ ,  $h_{rand} = 2$  (right) using a system length of  $L = 16$ . Similar to [5], we take the middle 70 percent of the energy eigenvalues for the calculation, as the eigenvalues at the ends of the spectra are sparse.

Figure 4 displays the results, and we can see that the relationship between the expectation values of operators and energies of eigenstates is approximately functional for a chaotic system, and non-functional for an integrable system. We can observe especially with the global operators  $T$  and  $Z$  a great deal of fine structure. There is still some variance, and we hypothesize that this is due to the finite system size. The small variance instead of a perfect functional relationship is consistent with calculations for a similar spin chain from [5].

To support the hypothesis that the not fully functional relationship between the operator expectation value and the eigenstate energy is due to a finite system size, we investigate how the variance of the expectation values within small energy windows of  $\Delta E$  varies with an increasing lattice size. From Figure 5, we can observe that the operator variance approaches zero rapidly with increasing  $L$  for the chaotic system, and is much larger for the integrable system.

## 5.6 Thermalization test

The ETH also states that the long-time average of expectation values of quantum operators should reproduce those computed using a microcanonical

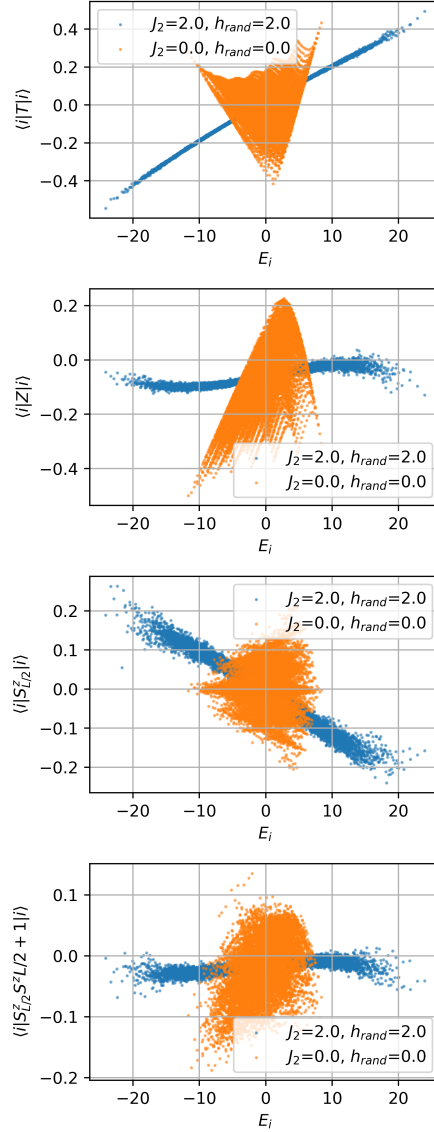


Figure 4: Expectation values of four different operators for Hamiltonian eigenstates  $|i\rangle$ , plotted against the energies of the eigenstates  $E_i$ . The chaotic Hamiltonian displays a smooth functional relationship  $a(E)$ , whereas the Hamiltonian of the integrable system does not. The computations are performed on a system size of  $L = 15$ .

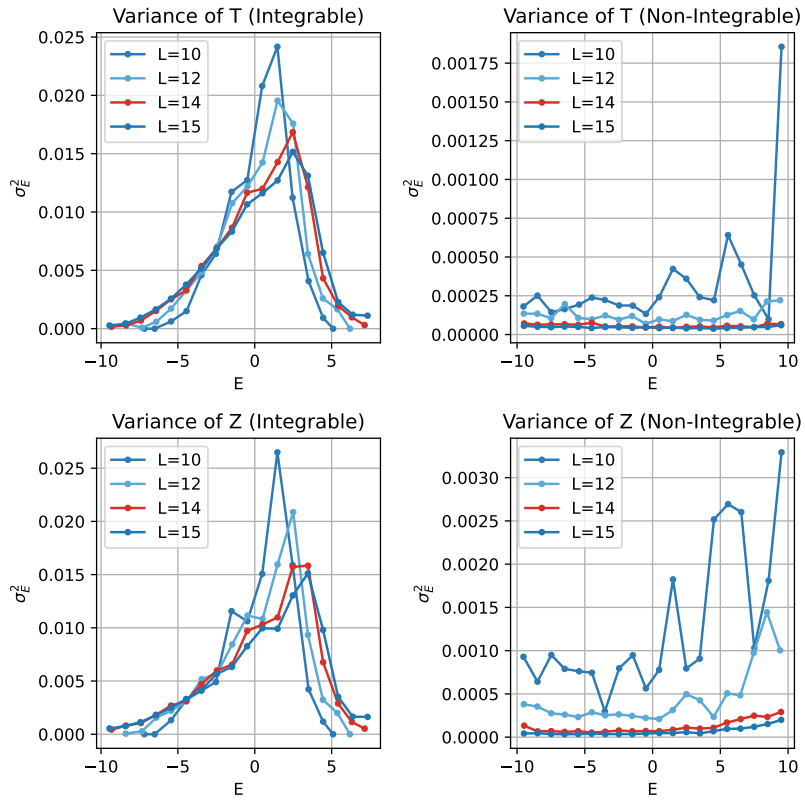


Figure 5: Variance of operators  $T$  and  $Z$  for an integrable system ( $J_2 = 0$ ,  $h_{rand} = 0$ ) and a chaotic system ( $J_2 = 2$ ,  $h_{rand} = 2$ ). The variance is computed for energy windows of  $\Delta E = 1$  for energies from  $-10$  to  $+10$ .

ensemble for non-integrable systems:

$$\langle A \rangle_\beta = \langle A \rangle_\infty \quad (22)$$

Let's define the partition function as

$$Z(\beta) = \sum_{\alpha} e^{-\beta E_{\alpha}}. \quad (23)$$

We can then compute the system inverse temperature for a given initial state  $\beta$  with energy  $E_0$  using bisection, looking for  $\beta \in [-10, 10]$ . More precisely, we are looking for such  $\beta$  that

$$\langle E \rangle_{thermal,\beta} \equiv \frac{\sum_{\alpha} E_{\alpha} e^{-\beta E_{\alpha}}}{Z(\beta)} = E_0, \quad (24)$$

where  $\alpha$  runs along the eigenstates.

Figure 7 displays the computed thermal average and the long-time quantum mechanical average. As we increase  $J_2$  from 0, the difference between the long-time quantum mechanical expectation value  $\langle A \rangle_\infty$  and the result obtained with a microcanonical ensemble  $\langle A \rangle_{thermal}$  grows smaller as the system transitions into chaotic behaviour.

To verify that this behavior is not special to the Néel state, we repeat the analysis for 1000 randomly generated product states from the same total magnetization sector. Figure 7 shows the distribution of the relative error  $(\langle Z \rangle_\infty - \langle Z \rangle_\beta)/\langle Z \rangle_\infty$ . For the integrable case ( $J_2 = 0$ ), the errors are broad and many fall far outside the displayed range, reflecting the failure of thermalization. For the chaotic case (large  $J_2$ ), the distribution is sharply peaked around zero, demonstrating that ETH successfully predicts the long-time behavior of local observables.

## 6 Conclusion

We have numerically demonstrated the Eigenstate Thermalization Hypothesis in a chaotic XXZ spin- $\frac{1}{2}$  chain and its breakdown for an integrable system.

Even though the Hamiltonians studied in this work are highly structured and far from random even for the chaotic case, we observed that their spectral statistics in the non-integrable regime coincide with those of random matrices

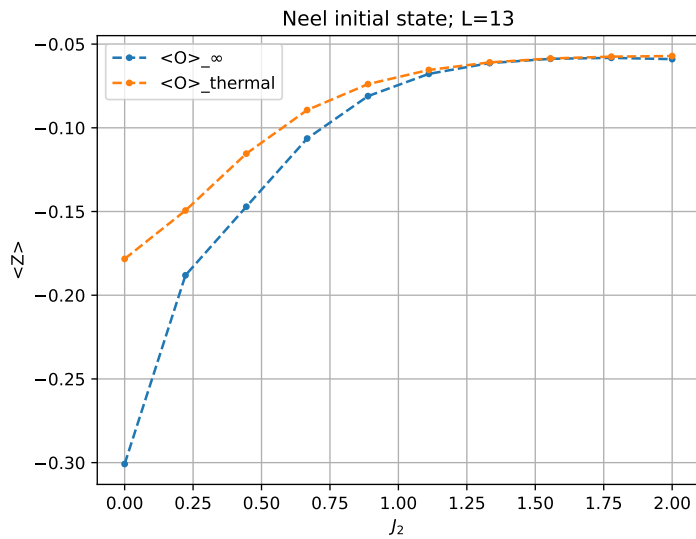


Figure 6: Comparison of the quantum mechanical operator expectation value  $\langle Z \rangle_\infty$  and the statistical mechanics-predicted operator expectation value  $\langle Z \rangle_{\text{thermal}}$  for various values of  $J_2$  (at  $h_{\text{rand}} = 0$ ). The initial state is the Néel state  $|\uparrow\downarrow\uparrow\downarrow\dots\rangle$ . The calculations were performed for a grid of size  $L = 13$ . As we enter the chaotic regime by increasing  $J_2$ , the difference between the two expectation values becomes smaller.

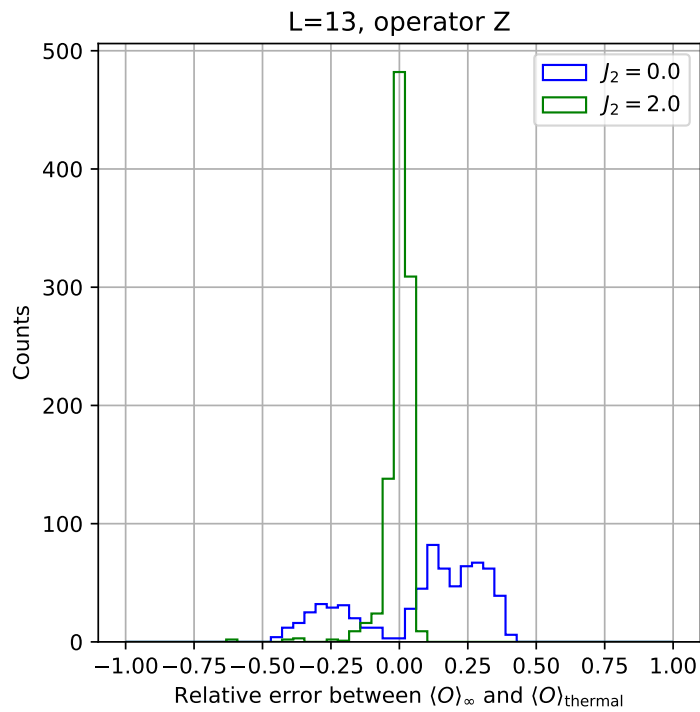


Figure 7: Distribution of the relative error  $\frac{\langle Z \rangle_\infty - \langle Z \rangle_{\text{thermal}}}{\langle Z \rangle_\infty}$  for two different values of  $J_2$ , for 1000 random initial states. Around 30% of the cases fall outside the displayed interval for the  $J_2 = 0$  case (integrable system).

of the Gaussian Orthogonal Ensemble universality class: We have shown that the spacings between energy levels for a chaotic quantum system respect the Wigner-Dyson distribution, a well-known result from Random Matrix Theory.

We have also shown that the expectation values of both local and global operators for different eigenstates form smooth function for a chaotic system and not for an integrable system. We attempted to explore the effects caused by a small, finite lattice size.

We could extend the results by having a larger lattice size; however, we are limited by compute power.

## Reproducibility

The code to reproduce these results is available at [https://github.com/gregorkrz/Eigenstate\\_Thermalization\\_Hypothesis](https://github.com/gregorkrz/Eigenstate_Thermalization_Hypothesis).

## AI statement

ChatGPT (GPT-5.1) was used to write parts of code, mainly the code for constructing the Hamiltonian and the basis space, as well as the other operators ( $T$ ,  $Z$ , local spin operators). The code was carefully checked to ensure correctness. The same model was also used to generate the more complex L<sup>A</sup>T<sub>E</sub>X formulas and improve grammar and coherence. Grammarly was also used to improve grammar.

## A Effect of the reflection symmetry breaking on the $J_2 = 0$ , $h_{rand} = 0$ case

Introducing the small magnetic field  $+\epsilon S_0^z$  to break the reflective symmetry of the XXZ model Hamiltonian does not significantly alter the Hamiltonian, as reflected in the distribution of the energy (eigenvalue) spacing in Figure 8: The distribution  $P(s)$  for this case remains exponential, demonstrating that introducing this small change doesn't significantly affect the system.

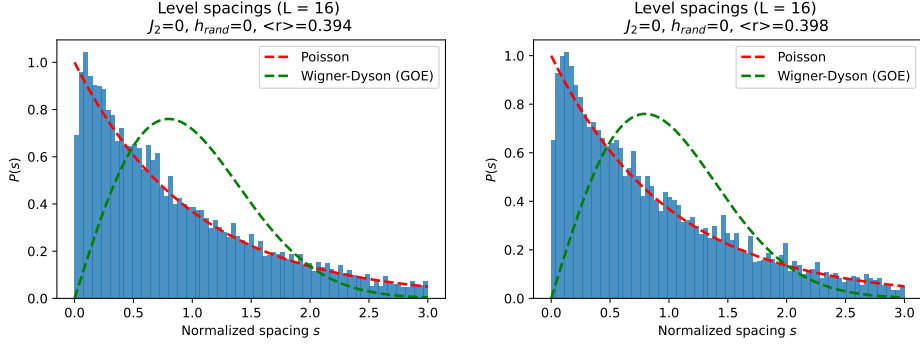


Figure 8: Distribution  $P(s)$  for the  $J_2 = 0$ ,  $h_i = 0$  case. The left figure is without the extra magnetic field at site 0, whereas the right figure includes the field without breaking the integrability of the system.

## References

- [1] V. E. Kravtsov. *Random matrix theory: Wigner-Dyson statistics and beyond. (Lecture notes of a course given at SISSA (Trieste, Italy))*. arXiv:0911.0639. Aug. 2012. DOI: 10.48550/arXiv.0911.0639. URL: <http://arxiv.org/abs/0911.0639> (visited on 10/27/2025).
- [2] Bernard Nienhuis and Onno E. Huijgen. *All local conserved quantities of the XXZ model*. arXiv:2104.01851. May 2021. DOI: 10.48550/arXiv.2104.01851. URL: <http://arxiv.org/abs/2104.01851> (visited on 11/26/2025).
- [3] Mark Srednicki. *Chaos and Quantum Thermalization*. arXiv:cond-mat/9403051. Apr. 1994. DOI: 10.48550/arXiv.cond-mat/9403051. URL: <http://arxiv.org/abs/cond-mat/9403051> (visited on 10/27/2025).
- [4] Lev Vidmar and Marcos Rigol. *Generalized Gibbs ensemble in integrable lattice models*. arXiv:1604.03990. June 2016. DOI: 10.48550/arXiv.1604.03990. URL: <http://arxiv.org/abs/1604.03990> (visited on 11/25/2025).
- [5] Ding-Zu Wang et al. *Eigenstate Thermalization and its breakdown in Quantum Spin Chains with Inhomogeneous Interactions*. arXiv:2310.19333. June 2025. DOI: 10.48550/arXiv.2310.19333. URL: <http://arxiv.org/abs/2310.19333> (visited on 11/25/2025).